Thermochimica Acta, 113 (1987) 53–66
Elsevier Science Publishers B.V., Amsterdam – Printed in The Netherlands

PREDICTOR–CORRECTOR NUMERICAL METHODS FOR KINETIC ANALYSIS OF TG DATA: METHODS APPLIED TO OIL SHALE PYROLYSIS

I.C. HOARE and W.I. STUART

CSIRO Division of Energy Chemistry, Lucas Heights Research Laboratories, Private Mail Bag 7, New South Wales 2232 (Australia)

(Received 24 July 1986)

ABSTRACT

Numerical methods were adapted for the direct solution of non-isothermal kinetic equations, and their use was illustrated by their application to the thermogravimetry of oil shale pyrolysis. Software packages were assembled for numerical integration using a predictor–corrector method, for graphical screen display of theoretical and experimental TG and DTG curves, and for refinement of kinetic parameters by non-linear regression. Experimental TG–DTG profiles were obtained for kerogen concentrates of two Australian oil shales, one being a torbanite from the historical deposit of Hartley Vale in New South Wales, and the other a brown shale from the Condor deposit in Queensland. No single kinetic model could be fitted to the experimental data, but functions based on multistage models gave excellent agreement between calculated and experimental TG–DTG profiles.

INTRODUCTION

There has been much discussion of methods for deriving kinetic parameters from non-isothermal data, and particularly from thermogravimetric and thermometric data. But although the principles of non-isothermal kinetic analysis have been thoroughly reviewed [1–4] (and in our view, are now well founded), their application is bedevilled by mathematical and computational problems.

In this paper, we show how some problems can be circumvented by using predictor–corrector numerical (PCN) methods combined with computer-generated screen graphics. The methods are demonstrated by kinetic analyses of the pyrolytic decomposition of kerogen (the organic component of oil shale).

BACKGROUND

TG and DTG measurements most often describe that class of reaction where a solid, on being heated at a constant rate $dT/dt = \beta$, decomposes to yield gaseous products.

0040-6031/87/$03.50

TABLE 1
Kinetic functions for solid decomposition

	Model	$g(\phi)$
F_1	1st order	ϕ
F_n	n-order	ϕ^n $n=1, n$
A_2	2-dimensional nucleation and growth (Avrami equation)	$2\phi[-\ln(\phi)]^{1/2}$
A_3	3-dimensional nucleation and growth (Avrami equation)	$3\phi[-\ln(\phi)]^{2/3}$
D_1	One-dimensional diffusion	$(1-\phi)^{-1}$
D_2	Two-dimensional diffusion	$[-\ln(\phi)]^{-1}$
D_3	Three-dimensional diffusion (Jander equation)	$\phi^{1/3}[\phi^{1/3}-1]^{-1}$
D_4	Three-dimensional diffusion (Ginstling–Brounshtein)	$[\phi^{-1/3}-1]^{-1}$
R_1	Phase boundary controlled, contracting cylinder	$\phi^{1/2}$
R_2	Phase boundary controlled, contracting sphere	$\phi^{2/3}$

Consider the simplest case of a one-stage transformation where decomposition of the solid is determined by a single mechanism.

The extent of decomposition at time t and temperature T is the mol fraction $1-\phi$, where ϕ, the mol fraction of unreacted solid, is calculated from the TG curve. Non-isothermal kinetic data are then described by

$$-d\phi/dT = (A/\beta)\, g(\phi) \exp(-E/RT) \quad (1)$$

where A and E are, respectively, the pre-exponential and energy kinetic parameters, and $g(\phi)$ is some function appropriate to the mechanism of decomposition.

Integration of eqn. 1 gives

$$\int d\phi/g(\phi) = (A/\beta)\int \exp(-E/RT)\, dT \quad (2)$$

Much work has been directed towards:

(i) evaluation of the Arrhenius integral $\int\exp(-E/RT)$, for which there is no analytical solution, although various approximate expressions have been proposed for its estimation [5–8];

(ii) establishing the most suitable form of $g(\phi)$ for a given system.

Table 1 lists commonly used forms of $g(\phi)$ and some solid-state kinetic models [3,9].

The function ϕ^n is often used for $g(\phi)$, and substitution in eqn. 1 then gives

$$-d\phi/dT = (A/\beta)\phi^n \exp(-E/RT) \quad (3)$$

Equation 3 can be linearized to

$$\ln(-d\phi/dT) = \ln A - \ln \beta + n \ln \phi - E/RT \quad (4)$$

and the parameters E, A and n may then be evaluated by fitting eqn. 4 to a set of experimental measurements using regression analysis.

In principle, the fitting of eqn. 3 directly to experimental data (that is, without recourse to linearization), can be treated as a non-linear regression problem with refinement of the parameters by a full-matrix least squares technique. This option, although statistically superior, is difficult to exercise because A is a large number (typically $10^{10} - 10^{20}$) and $\exp(-E/RT)$ is reciprocally very small; so successful first-guessing of kinetic parameters (that is, choosing values that lead to convergence of the regression program) is something of a lottery.

Occasions where thermal decomposition occurs through several reaction pathways, raise problems in thermokinetic analysis that have not been solved. Consider two examples:

(i) for thermal decomposition of a solid with i reactions proceeding concurrently we have for each reaction

$$-\mathrm{d}\phi_i/\mathrm{d}T = \mathrm{g}(\phi)(A_i/\beta)\exp(E_i/RT) \tag{5}$$

(ii) each reaction in a system of i independent reactions is described by

$$-\mathrm{d}\phi_i/\mathrm{d}T = \mathrm{g}_i(\phi_i)(A_i/\beta)\exp(E_i/RT) \tag{6}$$

In both cases the overall rate of reaction is given by

$$-\mathrm{d}\phi/\mathrm{d}T = \sum \mathrm{d}\phi_i/\mathrm{d}T \tag{7}$$

where $\phi = \Sigma\phi_i$

So eqn. 7 cannot be solved analytically. Clearly, numerical solutions to the rate equations are needed for a wider application of non-isothermal kinetic analysis. We have therefore assembled software routines that can be applied to a range of thermokinetic problems of varying complexity. The software serves three purposes.

(i) Direct solution of non-isothermal kinetic expressions, using the Gear predictor–corrector method [10] for the solution of systems of ordinary differential equations of the form $y' = \mathrm{f}(x, y)$.

(ii) Rapid screen-graphical display for comparing calculated and experimental TG and DTG curves.

(iii) Iterative refinement of kinetic parameters using non-linear regression.

The application of these numerical methods to thermokinetic analysis brings the following advantages.

(i) The Arrhenius integral $\int\exp(-\mathrm{E/RT})$ can be evaluated directly without the need for approximations.

(ii) A direct solution of $\mathrm{G}(\phi) = \int\mathrm{d}\phi/\mathrm{g}(\phi)$ can be obtained. This means that the choice of $\mathrm{g}(\phi)$ need no longer be restricted to those functions that provide an analytical solution of $\mathrm{G}(\phi)$.

(iii) Calculated TG and DTG curves can be rapidly generated and displayed on-screen. Thus a great deal of graphical experimentation can be carried out quickly, in order to judge the most appropriate kinetic model and then obtain a first estimate of kinetic parameters.

(iv) After the initial graphical assessment, the program is virtually one-step with iterative refinement of kinetic parameters by non-linear regression.
(v) The program is not confined to simple systems.

EXPERIMENTAL

A specimen of oil shale from the Condor deposit (Queensland) was supplied by Southern Pacific Petroleum P/L. The torbanite specimen was acquired by fossicking the historical oil shale workings at Hartley Vale in New South Wales. After crushing and sieving each sample, a sieved fraction (-1.4 to $+0.6$ mm) was ballmilled, and the resultant powdered material was used for all experiments. Kerogen concentrates were obtained by demineralisation with HCl then HF solutions.

TG data were obtained using a Cahn RG Electrobalance interfaced to an LSI-11/02 computer via a 12-bit A/D converter. Kinetic analysis of processed data was carried out on an IBM 4381 mainframe computer. DTA data were obtained using a Perkin-Elmer DTA 1700 thermal analyzer.

RESULTS AND DISCUSSION

Pyrolytic decomposition of kerogen: general features

Kerogen is formed by geochemical reactions involving organic debris of algae, spores, bacteria or higher plants. A commonly accepted model is that of a polymeric material composed of non-repeating polynuclear aromatic units with peripheral and bridging functional groups. The principal functional groups are alkyl and alkyl/aryl chain substituents and carboxylic groups.

Pyrolysis of kerogen is chemically complex in the sense that functional groups decompose to yield, inter alia, oil and combustible gas, each with a multitude of molecular constituents. However, it can be inferred from thermal analysis and infrared spectrophotometry [11–16] that thermal breakdown of kerogen in Australian oil shales, embodies three broad classes of reaction. These are as follows.

(1) Decarboxylation reactions (involving principally the decomposition of –COOH groups) that occur between about 100 and 450°C.
(2) The greatest mass loss and highest rates of decomposition occur between 400 and 650°C, and signal a major breakdown of kerogen to form oil and gas, with hydrocarbons as the main products. All aliphatic and some aromatic moieties are removed from the solid phase, leaving a wholly aromatic char. The composition of pyrolysates broadly relate to the composition of the parent kerogen, at least in terms of the yield of aromatic and normal hydrocarbons.

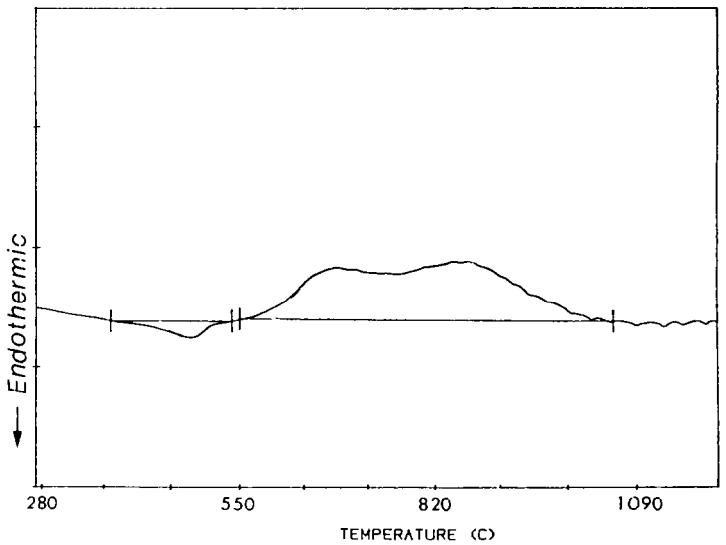

Fig. 1. DTA curve for Hartley Vale torbanite kerogen heated 10 °C min^{-1} in argon.

(3) Carbonization of the aromatic char occurs between about 500 and 1200 °C with evolution of hydrogen. This process, although contributing very little to the total mass loss, is accompanied by a substantial exothermic effect, exemplified by the DTA curve in Fig. 1.

The three processes cannot be distinguished as resolved steps and peaks in the TG and DTG pyrolysis curves.

Comparison of two Australian oil shales: composition and pyrolysis

Infrared absorption bands of kerogen give information about compositional features such as aromaticity and –COOH content. Differences in composition are highlighted in Fig. 2 which shows IR spectra for the kerogen concentrates. The two spectra are the same in the sense that they display the same major absorption bands, but differ considerably in the intensity of the various bands. The aliphatic content of Hartley Vale torbanite (HVT) kerogen is greater than that of the Condor material, as shown by the dominating alkyl bands at 2930, 2860 and 1464 cm^{-1}. The Condor material by contrast is the more aromatic as indicated by a strong 1620 cm^{-1} band, and contains a higher amount of –COOH groups with an intense C=O band at 1700 cm^{-1} and substantial O–H stretching band.

Analyses of pyrolysates from Australian torbanites and Condor oil shale suggest that compositional differences between the two kerogens are reflected in the composition of thermal degradation products. GC-pyrograms of Australian torbanites are dominated by normal hydrocarbons [17,18]. On the other hand, the composition of Condor pyrolysate, as indicated by the

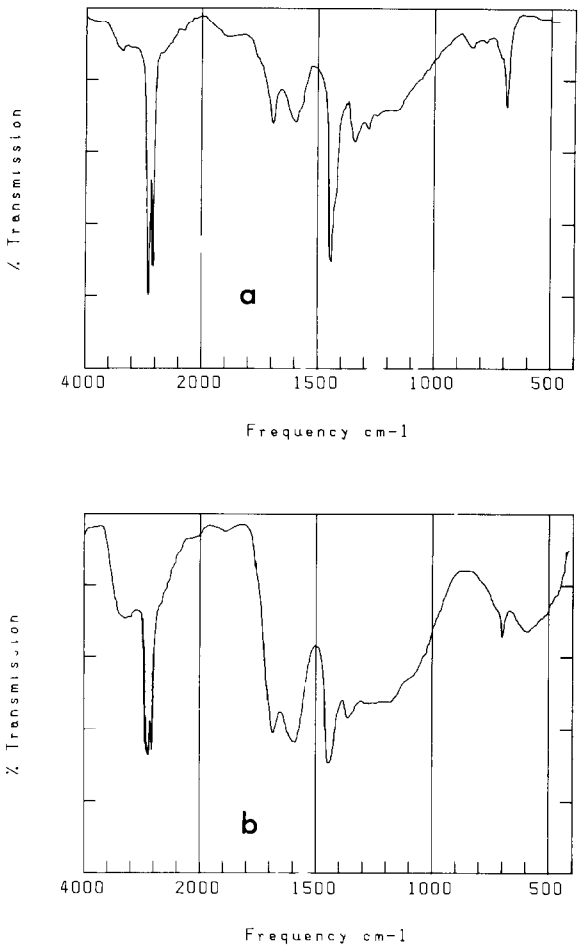

Fig. 2. Infrared spectra of kerogens: (a) Hartley Vale; (b) Condor.

analysis of Rovere et al. [19], is that of a highly aliphatic material, which nevertheless contains significant amounts of substituted aromatic compounds and nitriles.

Composition can also be related to TG–DTG pyrolysis profiles of the two kerogens, as shown in Fig. 3. HVT kerogen exhibits a sharper TG–DTG profile, with the principal mass loss occurring between 400 and 500°C, although the onset of mass loss is at 150°C. On the other hand, the TG–DTG profile is much broader for pyrolysis of Condor kerogen. Decomposition of carboxylic acid groups dominates the early stages of pyrolysis; so the higher concentration of –COOH groups found in the Condor kerogen account for the higher mass losses observed for this material between 150 and 400°C. The much broader DTG peak for Condor as compared to that for HVT kerogen, signifies a radical difference in kinetic behaviour for the

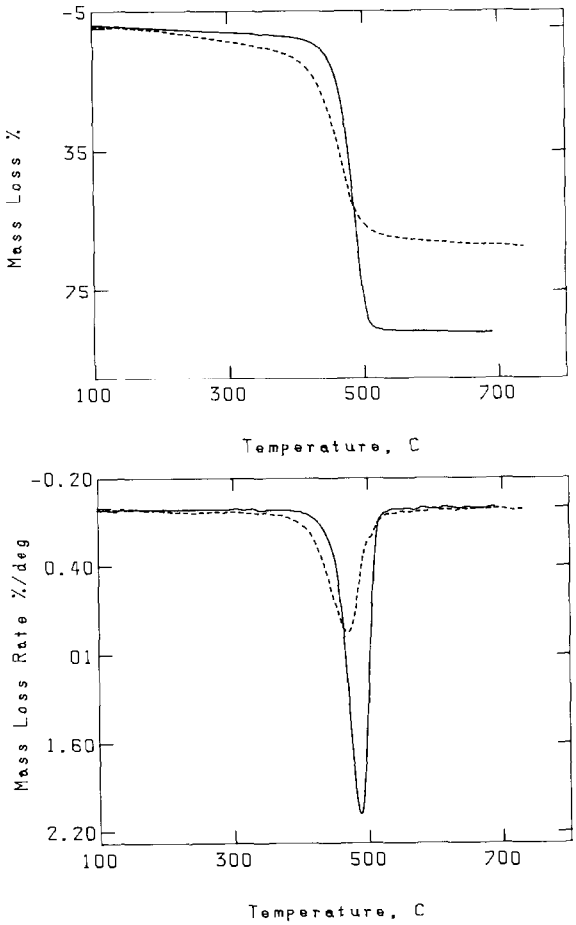

Fig. 3. TG–DTG pyrolysis profiles for kerogens heated in nitrogen at 10 °C min^{-1}. (———) Hartley Vale; (------) Condor.

second stage of pyrolysis. This difference is defined more precisely by thermokinetic analysis (vide infra).

Kinetic analysis: pyrolysis of Hartley Vale kerogen

Figure 4 depicts a series of calculated TG and DTG curves for $g(\phi) = \phi$ and for various values of the parameters A and E. The theoretical curves are compared with experimental data for HVT kerogen heated at 10 °C min^{-1}. The following can be seen.

(i) The main effect of varying either A or E is to displace the calculated TG curve along the temperature axis.

(ii) A first order expression can be fitted to the main part of the TG–DTG curves. Regression analysis showed that the best fit (as indicated by r-factor)

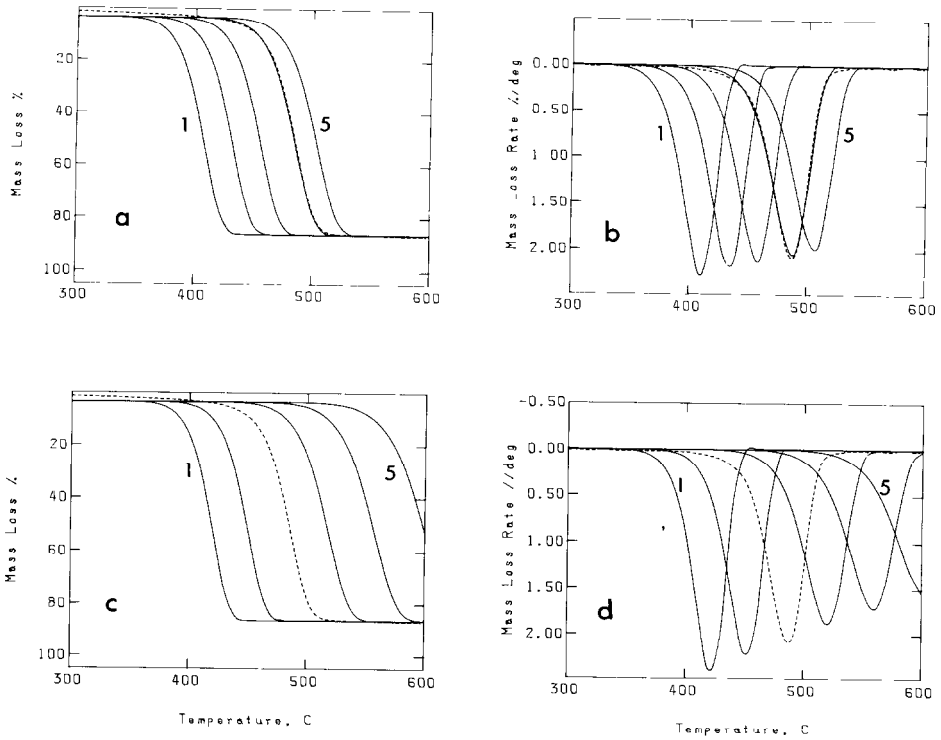

Fig. 4. (------) Experimental TG–DTG data for Hartley Vale kerogen heated 10 °C min^{-1} in nitrogen. (———) Calculated for $g(\phi) = \phi$ with kinetic parameters as follows: (a) and (b): effect of varying E, with $A = 1.8 \times 10^{21}$, E increasing from 280 kJ mol^{-1} (curve 1) to 320 kJ mol^{-1} (curve 5) in increments of 10 kJ mol^{-1}; (c) and (d): effect of varying A, with $E = 311$ kJ mol^{-1}, A increasing from 1.8×10^{18} (curve 1) to 1.8×10^{23} min^{-1} (curve 5) in single order increments.

TABLE 2
Pyrolysis of Hartley Vale Torbanite kerogen: kinetic models and parameters

Heating rate (°C min^{-1})	Extent of reaction $1 - \phi$	Model	n	A (min^{-1})	E (kJ mol^{-1})	r-factor
3	0–0.04	D4	–	0.12	30	8.8×10^{-6}
	0.04–0.08	D2	–	2.0×10^{12}	208	
	0.08–0.99	F1	1.0	2.5×10^{21}	311	
	0.99	D4	–	1.2×10	27	
10		D4	–	0.13	27	5.5×10^{-6}
		D2	–	2.2×10^{12}	208	
		F1	0.98	1.6×10^{21}	311	
		D4	–	1.3×10	23	
15		D4	–	0.10	23	3.1×10^{-6}
		D2	–	2.5×10^{12}	208	
		F1	0.97	1.5×10^{21}	312	
		D4	–	1.3×10	19	

is obtained by confining ϕ within the limits of 0.95 to 0.01.
(iii) There is a reproducible deviation of calculated and experimental data for the initial stage of pyrolysis (that is decarboxylation between 150 and 400°C). Likewise the final small mass loss arising from carbonisation at 550°C et seq. cannot be fitted by a simple *n*-order expression.

Further experimentation using PCN methods showed that the models based on diffusion-controlled processes give the best fit to the experimental data for the initial (decarboxylation) and final (carbonisation) stages of decomposition. There is then exceptionally good agreement between experimental data and the plots calculated using multistage kinetic models. The excellent fit of theoretical curves to experimental data is typified by the TG–DTG profiles in Fig. 5. Table 2 lists details of the kinetic models,

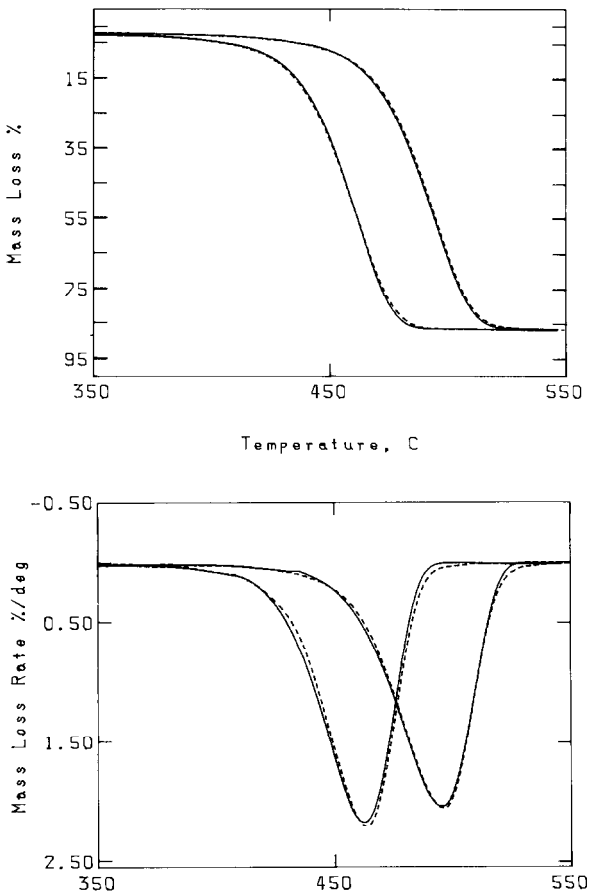

Fig. 5. TG–DTG pyrolysis profile of Hartley Vale kerogen, heated 3°C min^{-1} in nitrogen. (------) Experimental; (———) calculated.

together with kinetic parameters and *r*-factors computed iteratively for three experimental heating rates.

Kinetic analysis: pyrolysis of Condor kerogen

In the same way as for HVT kerogen, diffusion models give the best fit to both the initial and final sections of TG curves for Condor kerogen. On the other hand, second-stage pyrolysis of Condor kerogen follows a kinetic mode quite different from that of HVT kerogen. A simple function $g(\phi) = \phi^n$ cannot adequately be fitted to the experimental TG and DTG data. This can be seen in Fig. 6, where experimental TG and DTG curves are compared

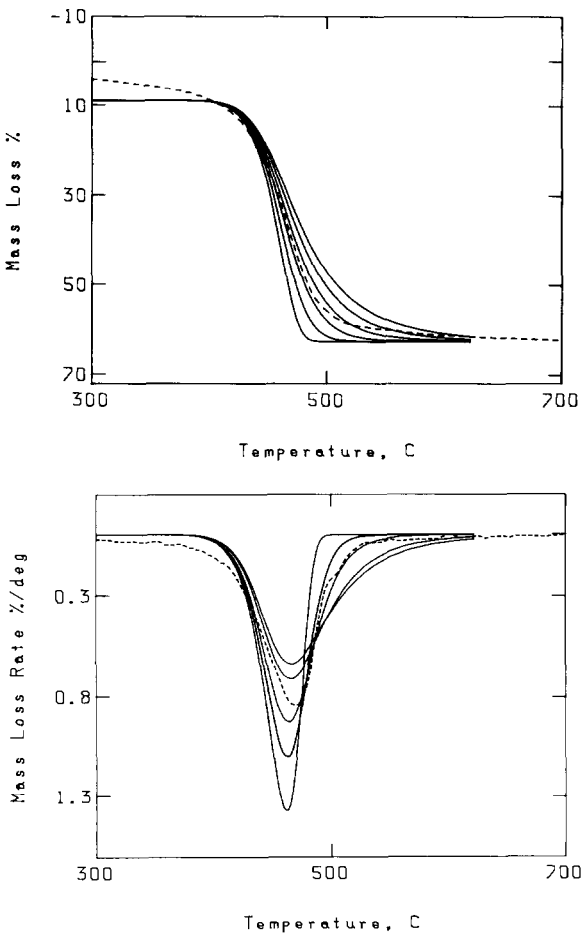

Fig. 6. (------) Experimental TG–DTG data for Condor kerogen heated 10 °C min^{-1} in nitrogen. (———) Calculated for $g(\phi) = \phi^n$, $E = 310$ kJ mol^{-1}; $A = 1.8 \times 10^{21}$ and values of n from 1.0 to 3.5 in increments of 0.5.

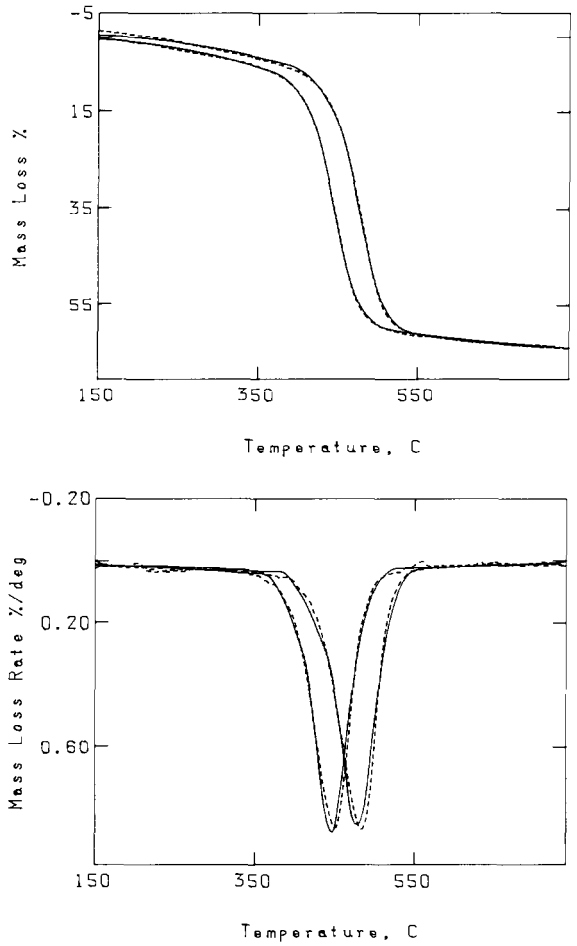

Fig. 7. TG–DTG pyrolysis profile for Condor kerogen heated in nitrogen at 4°C min^{-1}. (------) Experimental; (———) calculated using multi-kinetic model.

with several theoretical curves calculated by solving eqn. 3 for various values of the exponent n. Clearly the experimental data cannot be expressed in terms of eqn. 3, no matter what the value of n may be.

However, a very good fit to the experimental data can be obtained by adopting an equation for two concurrent, independent processes with each following F_n kinetics, that is:

$$d\phi/dt = (\phi_1)^n A_1 \exp(-E_1/RT) + (\phi_2)^m A_2 \exp(-E_2/RT) \quad (8)$$

In this case, PCN methods are essential for the solution of eqn. 8 and for the subsequent construction of calculated TG and DTG curves.

Figure 7 shows experimental TG and DTG curves for Condor kerogen heated at 4°C min^{-1}. Also shown are curves calculated by combining eqn. 8 with equations based on diffusion-controlled processes. It can be seen that

TABLE 3
Pyrolysis of Condor kerogen: kinetic models and parameters

Heating rate (°C min^{-1})	Extent of reaction $1-\phi$	Model	A (min^{-1})	E (kJ mol^{-1})	r-factor
4	0–0.09	D4	0.3	25	1.3×10^{-5}
	0.09–0.27	D2	6.5×10^{13}	209	
	0.27–0.94	F_n ($n=2.0$)	2.2×10^{21}	300	
		$+F_m$ ($m=3.1$)	1.4×10^{20}	310	
	> 0.94	D4	4.3	28	
10		D4	0.9	26	8.3×10^{-6}
		D2	5.2×10^{13}	210	
		F_n ($n=2.0$)	1.6×10^{21}	301	
		$+F_m$ ($m=3.1$)	0.8×10^{19}	312	
		D4	4.9	25	
20		D4	1.4	27	8.3×10^{-6}
		D2	5.2×10^{13}	210	
		F_n ($n=1.9$)	1.1×10^{21}	300	
		$+F_m$ ($m=3.1$)	3.1×10^{19}	315	
		D4	11	21	

this combination provides a very satisfactory fit to the experimental data throughout the entire range of ϕ.
Three sets of kinetic parameters are given in Table 3 for Condor kerogen. These were derived by fitting the multistage kinetic model to experimental TG data measured at different heating rates.

The exercises that we have described, are primarily examples of curve-fitting of well-known kinetic functions to experimental TG–DTG profiles, using a rather novel approach to kinetic analysis of thermogravimetric data. The results show that PCN methods are invaluable for rapidly generating theoretical TG and DTG curves. The methods are particularly serviceable in the case of a complex system where the integral function $G(\phi)$ cannot be evaluated analytically, as can be seen by the description of Condor data in terms of two concurrent independent processes.

Although the work was principally an exploration of PCN methods and their application, there is nevertheless a correspondence between the kinetic functions and the properties of the two kerogens that, broadly, makes chemical sense: the two kerogens differ in composition; the oil pyrolysates are chemically different; and kinetic functions required to describe second-stage pyrolysis are likewise different. This is strong evidence that the second stage of pyrolytic decomposition is kinetically controlled by bond rupture. By contrast, the first and final stages of pyrolysis are chemically non-specific and diffusion-controlled. These findings are in general accord with the results of Lynch and Webster [20] who used ^{1}H-NMR thermal scanning methods to show how the proportion of "mobile" and "rigid" H varies

during pyrolysis of kerogen. Their results indicate that, during decarboxylation, kerogen is in the form of a rigid solid; a transient softening then occurs during the main stage of pyrolysis, leading to a rigid aromatic char. Diffusion-controlled mechanisms for both the first and final stages of pyrolysis are, therefore, consistent with these findings.

Questions still remain; for example, even though there is an excellent fit of the simple function $g(\phi) = \phi$ to second-stage pyrolysis of HVT kerogen, this stage is not by any means a simple reaction. There are many different products of decomposition which for Australian torbanites are predominantly normal hydrocarbons [16,17]. This dilemma can be resolved by assuming that, for HVT kerogen, the second and major pyrolytic stage encompasses a series of parallel reactions, with the rate of each reaction described by

$$-\mathrm{d}\phi_i/\mathrm{d}T = (\phi/\beta)A_i\exp(-E_i/RT) \tag{9}$$

so if E_e and A_e are the kinetic parameters derived from experimental data, then

$$A_e\exp(-E_e/RT) = \sum A_i\exp(-E_i/RT) \tag{10}$$

from which we can deduce that

$$A_i\exp(-E_i/RT) = A_j\exp(-E_j/RT) = \ \ldots \text{ for all } i,\ j \tag{11}$$

which implies that, at least for HVT kerogen, the compensation effect operates throughout the second stage of pyrolysis. This is feasible. From chromatographic and IR spectral evidence, we can say that this stage is predominantly thermal excision of aliphatic groups to yield n-hydrocarbon pyrolysates; that is, the various decomposition reactions amount to a homologous series.

The chemical structure of Condor kerogen and its complex pyrolysate composition suggest that a compensation effect in this case cannot be invoked. So it is not clear at this time, whether the fit of eqn. 8 to second-stage pyrolysis denotes some as yet unrecognised mechanism, or fortuitously, a system of parallel first-order decomposition reactions where the compensation effect does not apply.

The general approach outlined in this paper is thought to be a necessary step in the solution of many problems in the field of non-isothermal kinetics; it is a means of exploring new and improved kinetic models involving more complex functions than have been used hitherto.

REFERENCES

1 J.H. Flynn and L.A. Wall, J. Res. NBS, 70A (1966) 487.
2 J. Sestak, V. Satava and W.W. Wendlandt, Thermochim. Acta, 7 (1973) 333.

3 W.E. Brown, D. Dollimore and A.K. Galwey, Comprehensive Chemical Kinetics, Vol. 22, Elsevier, Amsterdam, 1980.
4 E. Koch, Non-Isothermal Reaction Analysis, Academic Press, New York, 1977.
5 H.H. Horowitz and G. Metzger, Anal. Chem., 35 (1963) 1464.
6 A.W. Coats and J.P. Redfern, Nature (London), 201 (1964) 68.
7 A. Briodo and F.A. Williams, Thermochim. Acta, 6 (1973) 245.
8 G.I. Senum and R.T. Yang, J. Therm. Anal., 11 (1977) 445.
9 J.P. Elder, Thermochim. Acta, 95 (1985) 41.
10 C.W. Gear, Numerical Initial Value Problems in Ordinary Differential Equations, Prentice-Hall, Englewood Cliffs, NJ, 1971.
11 W.I. Stuart and J.H. Levy, Thermochim. Acta, 74 (1984) 227.
12 J.H. Levy and W.I. Stuart, Proceedings, First Australian Workshop on Oil Shale, Lucas Heights, Australia, May 18–19, 1983.
13 J.H. Levy and W.I. Stuart, Proceedings, Second Australian Workshop on Oil Shale, St. Lucia, Australia, December 6–7, 1984.
14 W.I. Stuart and J.H. Levy, Proceedings of the 14th Conference of the North American Thermal Analysis Society, San Francisco, September 15–18, 1985.
15 H.J. Hurst and A. Ekstrom, Proceedings of the Second Australian Workshop on Oil Shale, St. Lucia, Australia, December 6–7, 1984.
16 A. Ekstrom, H.J. Hurst and C.H. Randall, in F.P. Mikris and J.F. McKay (Eds.), Geochemistry and Chemistry of Oil Shales, ACS Symposium Ser. 230, Am. Chem. Soc., Washington, 1983.
17 S.R. Larter, in K.J. Voorhees (Ed.), Analytical Pyrolysis, Butterworths, London, 1984.
18 S.R. Larter and J.T. Senftle, Nature (London), 318 (1985) 277.
19 C.E. Rovere, P.T. Crisp, J. Ellis and P.D. Bolton, Fuel, 62 (1983) 1275.
20 L.J. Lynch and D.S. Webster, in F.P. Mikris and J.F. McKay (Eds.), Geochemistry and Chemistry of Oil Shales, ACS Symposium Ser. 230, Am. Chem. Soc., Washington, 1983.